PHYSICAL REVIEW B VOLUME 26, NUMBER 10 15 NOVEMBER 1982

Charge-density-wave transport in orthorhombic TaS_3. II. Frequency-dependent conductivity

A. Zettl, C. M. Jackson, and G. Grüner
Department of Physics, University of California at Los Angeles, Los Angeles, California 90024
(Received 16 April 1982)

Frequency- (ω) dependent conductivity measurements are reported on the linear-chain compound orthorhombic TaS_3. A weak frequency dependence and positive dielectric constant are observed due to one-dimensional fluctuations of charge-density waves (CDW's) above the Peierls transition at $T_P=215$ K. Below the phase transition the conductivity strongly increases with increasing ω, and the dielectric constant is of the order of 10^7. The small characteristic energies obtained from the observed ω dependence give direct evidence for the collective mode. When interpreted in terms of a classical model of the pinned CDW, $\sigma(\omega)$ indicates a strongly overdamped response. A tunneling model developed by Bardeen also leads to a consistent description of both $\sigma(\omega)$ and the electric-field- (E) dependent dc conductivity $\sigma(E)$. In this model the frequency-dependent response is due to both a tunneling contribution and the response of the pinned mode. Below about 130 K the observed frequency dependence suggests the development of a disordered CDW state. These observations are compared with experiments performed on the linear-chain compound $NbSe_3$.

I. INTRODUCTION

In the preceding publication[1] (hereafter referred to as I) we have reported the observation of strongly electric-field- (E) dependent conductivity $\sigma(E)$ in the charge-density-wave (CDW) state of the linear-chain compound orthorhombic TaS_3. The nonlinear conductivity provides clear evidence for charge transport carried by a collective mode, the sliding charge-density wave, a mechanism suggested by Fröhlich[2] more than 20 years ago. While various phenomenological models[3] can qualitatively describe the main features of the nonlinear transport (in particular the appearance of a sharp threshold field and the saturation of the conductivity at high electric fields), detailed fits suggest a tunneling[4,5] mechanism. The low electric field strengths which characterize the field-dependent conductivity suggest small pinning energies for the CDW and enormous characteristic lengths (of the order of microns) involved in the problem. At low temperatures, the coherent response of the CDW is not observed and we argued that, because of the absence of coupling between CDW segments, a disordered CDW state develops. The conductivity is also nonmetallic (i.e., σ decreases with decreasing temperature) above the phase transition $T_P=215$ K, and we have suggested that one-dimensional (1D) fluctuations are responsible for this behavior.

In this paper we report the observation of strongly frequency- (ω) dependent conductivity and giant dielectric constant ϵ in the CDW state of orthorhombic TaS_3. Both represent small energies associated with the pinning of the CDW. The frequency-dependent conductivity, when interpreted in terms of a classical description, suggests an overdamped response. Analysis in terms of Bardeen's tunneling model[4,5] accounts for both the field- and frequency-dependent response, with parameters similar to those observed in the linear chain compound $NbSe_3$. At low temperatures disorder effects are evident in the ω-dependent conductivity.

Frequency-dependent conductivity and a positive dielectric constant are also observed above the Peierls transition, although both are much less pronounced than in the CDW state below T_P. This provides further evidence for the 1D resistive fluctuations above T_P and for the dynamic localization which sets in as a consequence of the buildup of 1D correlations.

This paper is organized as follows: In Sec. II we describe the experimental techniques which were used to study the frequency dependence of the conductivity. In Sec. III we present our experimental results. This is followed by a discussion in Sec. IV. A comparison with $NbSe_3$ in Sec. V is followed by

the conclusion. Parts of our experiments were published earlier.[6,7]

II. EXPERIMENTAL TECHNIQUES

TaS_3 samples used for the frequency-dependent conductivity measurements were from the same preparation batch from which specimens for the field-dependent conductivity measurements were selected. Powder x-ray measurements[1] confirm that the samples have the orthorhombic form.

We have used three experimental methods to determine $\sigma(\omega)$ described in this report. In all cases $\omega/2\pi$ denotes both the frequency at which the sample was driven and the frequency at which the response was detected. Our methods allow simultaneous measurement of the in-phase and out-of-phase components of the conductivity, $\mathrm{Re}\sigma(\omega)$ and $\mathrm{Im}\sigma(\omega)$. Between 4 MHz and 2.4 GHz a HP 8754A network analyzer was used to determine $\sigma(\omega)$. The measurement technique involved directly terminating a 50-Ω coaxial cable with a TaS_3 crystal, and then measuring the return loss of the cable termination with the network analyzer. $\sigma(\omega)$ was easily extracted from the complex return loss with the aid of a straightforward computer program. A built-in network analyzer circuit, which compensated for the finite cable length between the sample and the measuring port, allowed a continuous variation of the frequency between 4 and approximately 500 MHz. Measurements at 1 and 2.4 GHz used a cable length fixed at $\lambda/2$, where λ is the wavelength of the excitation wave, and for these frequencies ω was held constant during the experimental run, and only the temperature was varied. A second measurement method, operational between 5 and 100 MHz, used an active rf bridge circuit developed by us. In this method the TaS_3 sample was balanced by a parallel-combination variable resistance and capacitance. The values of the balance resistance and capacitance, for a null bridge output, were then used to compute $\mathrm{Re}\sigma(\omega)$ and $\mathrm{Im}\sigma(\omega)$ for the sample. Both the network analyzer and bridge methods used two-probe sample mounting configurations, and contacts were made with conductive silver paint. Careful comparisons between these two-probe measurements at $\omega=0$ and separate four-probe dc measurements showed a contact resistance at room temperature more than 2 orders of magnitude less than the sample resistance, and an even better ratio at lower temperatures.

Because of the short length (between 5 and 10 cm) of the coaxial cable used between sample and measuring device for both above experimental methods, a specially designed ^{4}He gas-flow system was used to vary the temperature. This system had a temperature accuracy of about 1 K and a stability better than 0.1 K at all temperatures.

Microwave measurements at 9.14 GHz used the contactless cavity perturbation technique of Burovov and Shchegolev.[8] The complex dielectric constant of the sample was determined from the normalized frequency shift (δ) and change in Q (Δ) of a resonant cavity, obtained by inserting the sample into and removing it from the cavity. The sample was placed in a node of E-field maximum, oriented with the long axis parallel to the E field in a TE_{011} mode of a cylindrical cavity. An HP 8620C x-band sweeper was used to drive the frequency through resonance, and a significant improvement in the signal-to-noise ratio was achieved for the data by using a multichannel signal averager, triggered by a reference cavity. The sample cavity was placed in a standard ^{4}He cryostat with a long-term temperature stability better than 1 K.

In the microwave analysis, the complex dielectric function $\epsilon^*=\epsilon'-i\epsilon''$ is related to δ and Δ by

$$\epsilon'-1=\frac{1}{n}\frac{\delta\left[\frac{1}{n}-\delta\right]-\left[\frac{\Delta}{2}\right]^2}{\left[\frac{\Delta}{2}\right]^2+\left[\frac{\alpha}{n}-\delta\right]^2} \tag{1}$$

and

$$\epsilon''=\frac{\alpha}{n^2}\frac{\left[\frac{\Delta}{2}\right]}{\left[\frac{\Delta}{2}\right]^2+\left[\frac{\alpha}{n}-\delta\right]^2}, \tag{2}$$

where α is the filling factor and n the depolarization factor. $\mathrm{Re}\sigma(\omega)$ and $\mathrm{Im}\sigma(\omega)$ are related to ϵ^* by $\mathrm{Re}\sigma(\omega)=\epsilon_0\omega\epsilon''$ and $\mathrm{Im}\sigma(\omega)=\epsilon'-1$. Because of the fiborous morphology of the TaS_3 crystals, an accurate determination of the exact value of the conductivity at 9.1 GHz was not possible, and we have therefore expressed our data normalized to the room-temperature results. In order to insure the validity of the quasistatic analysis of Burovov and Shchegolev,[8] special care was taken to choose samples which were much smaller in diameter than the classical skin depth at 9 GHz.

Typical crystal dimensions were 1 μm$\times$10 μm$\times$0.5 mm for the rf measurements and 1 μm$\times$10 μm$\times$2 mm for the cavity microwave measurements. The long dimensions correspond to the chain axis in TaS_3, and all $\sigma(\omega)$ measurements re-

ported here are with respect to this chain direction. Owing to the inherent nonlinear dc transport properties observed in TaS_3, it is important to keep the amplitude of the ac driving field as small as possible. In all measurements the ac amplitude V_{ac} was at least 1 order of magnitude smaller than the threshold voltage V_T for the onset of nonlinear dc conductivity. Occasional checks were made to ensure that the measured ac conductivity $\sigma(\omega)$ was independent of V_{ac}, as expected for the small-perturbation limit. We therefore believe that our $\sigma(\omega)$ measurements are an accurate representation of the $V_{ac} \rightarrow 0$ limit.

III. EXPERIMENTAL RESULTS

The conductivity measured at dc, 2.4, and 9.1 GHz, is shown in Fig. 1 in the σ vs $1/T$ representation. No frequency dependence is found at high temperatures, where the dc conductivity displays a metallic behavior, while in the semiconducting state a strongly frequency-dependent conductivity is found, and σ measured in the GHz frequency region at low temperatures is orders of magnitude larger than the dc conductivity. Figure 2 shows the high-temperature behavior of the conductivity in more detail. The frequency-independent conductivity observed down to approximately 240 K is followed by a well-defined frequency dependence which becomes more pronounced as the temperature decreases, and while the dc conductivity sharply decreases, the 9.1-GHz conductivity is (within experimental error) independent of T. For completeness, we show the measured values of δ and Δ, used in the 9.1-GHz conductivity analysis, in Fig. 3. The onset of the phase transition at $T_P = 215$ K is signaled by the appearance of a frequency dependence which is more pronounced below T_P. This is

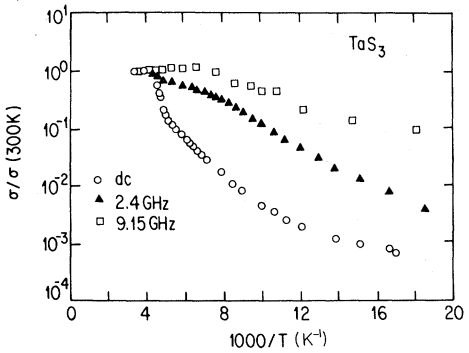

FIG. 1. Temperature dependence of the conductivity of orthorhombic TaS_3 at various frequencies.

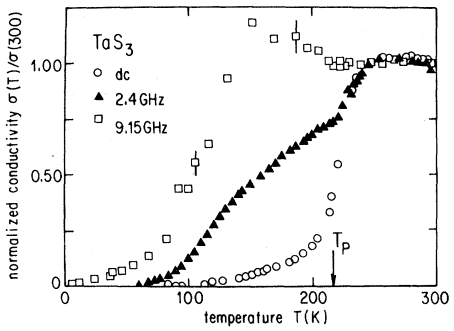

FIG. 2. Temperature dependence of the conductivity of TaS_3 at various frequencies.

evidenced by a sharp change of the slope $d\sigma/dT$ measured at 2.4 GHz. The 9.1-GHz conductivity increases with decreasing temperature down to about 150 K, but this may be an artifact of the analysis which neglects any influence of a finite skin depth at this frequency. Owing to these ambiguities, and the semiqualitative nature of this experimental data obtained at 9.1 GHz, we shall not use these data when $\sigma(\omega)$ is compared with the predictions of various models.

The frequency dependence of $\mathrm{Re}\sigma(\omega)$ and $\mathrm{Im}\sigma(\omega)$ measured at various temperatures below T_P is shown in Fig. 4. The experiments between 4 and 500 MHz were performed during the same experimental run, while the experimental points at 1.3 and 2.4 GHz were measured separately. $\mathrm{Re}\sigma(\omega)$ smoothly increases with increasing frequency, and there is an associated maximum in $\mathrm{Im}\sigma(\omega)$ at frequencies where $\mathrm{Re}\sigma(\omega)$ shows the strongest fre-

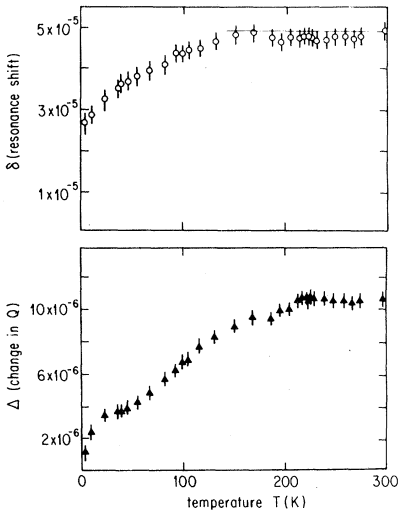

FIG. 3. Temperature dependence of the cavity shift and absorption in TaS_3 measured at 9.1 GHz.

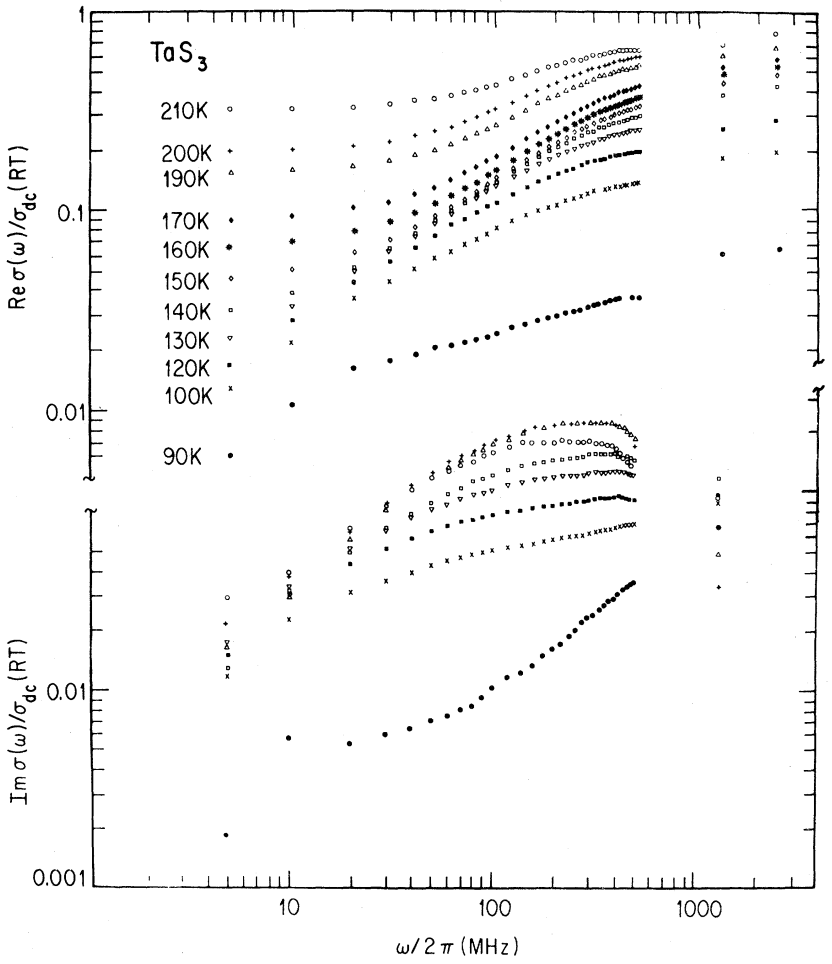

FIG. 4. Frequency dependence of the real and imaginary parts of the conductivity, $\mathrm{Re}\sigma(\omega)$ and $\mathrm{Im}\sigma(\omega)$, at various temperatures below $T_P=215$ K. The symbols for $\mathrm{Im}\sigma(\omega)$ refer to the same temperatures identified in the plot of $\mathrm{Re}\sigma(\omega)$.

quency dependence. In contrast to the field-dependent conductivity there is no threshold for the onset of frequency-dependent conductivity, and the frequency dependence extends to $\omega\rightarrow 0$. Below about 130 K, the frequency dependence becomes progressively more smeared with decreasing temperature, and we do not see a saturation of $\mathrm{Re}\sigma(\omega)$ or a maximum in $\mathrm{Im}\sigma(\omega)$, up to 2.4 GHz, in this temperature range.

At room temperature the dielectric constant ϵ is approximately equal to zero, while below T_P it is dramatically large. Figure 5 shows ϵ plotted as a function of temperature in the high-temperature region, for various frequencies. The phase transition at T_P is associated with a rapid increase in ϵ, and below 215 K ϵ is approximately independent of the temperature. While the dielectric constant is frequency dependent in the measured frequency range, this dependence is weak in the $\sim$10-MHz region. We assume, therefore, that ϵ measured at 10 MHz is close to the low-frequency dielectric constant, $\omega\rightarrow 0$.

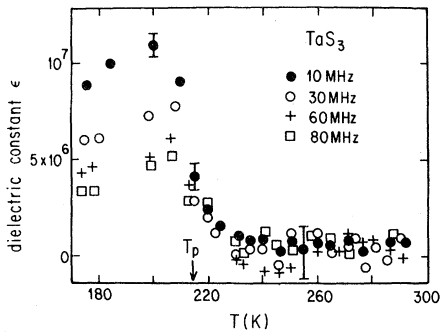

FIG. 5. Temperature dependence of the dielectric constant of TaS_3 measured at various frequencies. The transition temperature T_p is identified in the figure.

IV. DISCUSSION

The temperature dependence of the low-field dc conductivity, and the field-dependent conductivity discussed in I, indicated that CDW phenomena manifest themselves in three different temperature regions. The strong decrease of σ_{dc} below room temperature but above T_P was interpreted as evidence for 1D resistive fluctuations.[7] Below T_P but above approximately 100 K the sharp threshold field for the onset of dc nonlinearity was interpreted as due to the coherent response of the CDW to the external dc driving field. We also suggested that at low temperatures a disordered CDW state develops. In this section we interpret our experimental results and discuss the various temperature regions separately.

A. 1D fluctuation region, $T > T_P$

In the CDW fluctuating region, the progressive development of 1D correlations with decreasing temperature (evidenced by the appearance of diffuse streaks in the x-ray spectra[9]) leads to a gradual opening of a pseudogap around the Fermi surface. The subsequent decrease of the number of carriers which participate in the conduction process leads to a decrease of the dc conductivity, as observed. With this effect alone, one would observe a "metallic" conductivity, with current carried by an extended electron state. Consequently the conductivity would be independent of the frequency at frequencies $\hbar\omega < \Delta$ where Δ is a measure of the width of the pseudogap which develops above T_P. Also there would be no out-of-phase component to $\sigma(\omega)$ at frequencies $\hbar\omega < \Delta$. Both are in contrast to the experimental observations. In Fig. 6(a) we show the conductivity measured at 2.4 and 9.1 GHz, normalized to the dc conductivity measured at the same temperature, while Fig. 6(b) shows the dielectric constant measured at 10 MHz for the same temperature region. Both are in contrast to what is expected for band transport, and we suggest that localization effects are important in this temperature region.

Although a rigid division of the electron system into uncondensed electrons and electrons which build up the 1D correlations is somewhat arbitrary, we can visualize the effect of fluctuating 1D CDW segments as leading to random potentials seen by the uncondensed electrons. This random potential may lead to localization of the single-particle states,

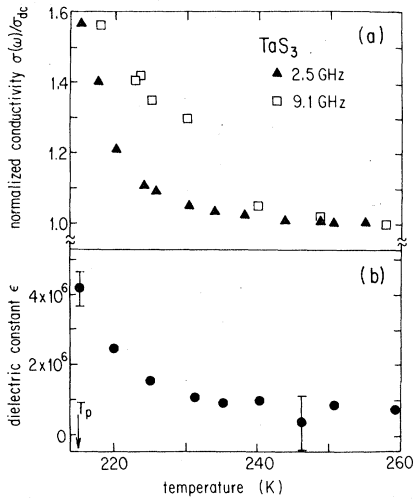

FIG. 6. (a) Temperature dependence of the normalized conductivity $\sigma(\omega)/\sigma_{dc}$ for TaS_3 above the Peierls transition. (b) Temperature dependence of the low-frequency ($\omega/2\pi = 10$ MHz) dielectric constant above the Peierls transition. The transition temperature T_p is identified in the figure.

and subsequently to frequency-dependent conductivity and a positive dielectric constant, as observed for highly anisotropic materials with static disorder.[10,11] Alternatively, $\sigma(\omega)$ and ϵ may reflect not the uncondensed electrons, but the response of the 1D CDW segments, which are pinned by residual impurities.

Either effect would lead to a frequency-dependent response and a positive dielectric constant which become more pronounced when T approaches T_P. Localization may become more important as the temperature approaches T_P from above, because the density of states at the Fermi surface, $N(0)$, decreases with the opening up of the pseudogap, and $N(0) \sim \xi^{-1}$ where ξ is the correlation distance of the 1D CDW's.[12] This suggests that the gradual buildup of 1D correlations will increase the number of normal electrons found in localized (single-particle) states, and consequently both $\sigma(\omega)$ and ϵ become more pronounced. Alternatively, since ξ is proportional to the number of electrons condensed in the 1D CDW mode, the dielectric constant and frequency response due to these modes will increase with ξ. In the absence of a detailed theory of the 1D Peierls-Frölich conductor we only note that both $\epsilon(\omega)$ and $\sigma(\omega)/\sigma(0)$ appear to have the same temperature dependence as $\xi(T)$, evaluated from diffuse x-ray experiments,[9] demonstrating the close correlation between struc-

tural evidences of 1D correlations and the associated anomalous transport phenomena.

B. Coherent CDW state below T_P

Below the Peierls transition the CDW on neighboring chains are correlated, leading to a 3D-ordered CDW state, as evidenced by x-ray studies.[9] Several models discuss the response of the CDW to external ac excitations. As discussed in I, both a classical[13,14] and quantum-mechanical[4,5] description account for the main qualitative features of the nonlinear conductivity, and a tunneling model[4,5] describes the field dependence in detail in the nonlinear region.

Before comparing our experimental findings with these theories we note that the frequency-dependent part of the conductivity is independent of the temperature between T_P and approximately 130 K. This is shown for the real part of the conductivity in Fig. 7, where we have subtracted the dc component of the conductivity from the measured $\mathrm{Re}\sigma(\omega)$. The temperature independence of the imaginary part of the conductivity for the same temperature range can be clearly seen in Fig. 4. Here a subtraction is not necessary, since, in the frequency range being considered, the uncondensed electrons do not give an out-of-phase component to the frequency-dependent response. We have also found that the field dependence of the dc conductivity $\sigma(E)$ is independent of the temperature in this region.[1,15]

Temperature-driven excitations therefore do not play an important role in the frequency- (and field-) dependent response. We therefore neglect the effect of finite temperature on the CDW response, and discuss only models where both $\sigma(\omega)$ and $\sigma(E)$ are accounted for at $T=0$. All of these models assume that at low electric field strength the CDW is pinned and does not contribute to the dc conductivity.

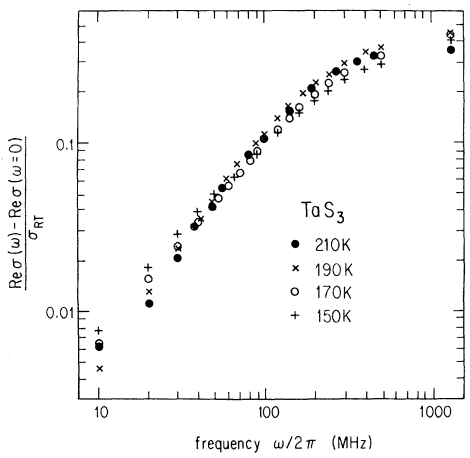

FIG. 7. Frequency dependence of the ac conductivity of TaS_3 at various temperatures. The dc conductivity has been subtracted in each case.

The frequency-dependent conductivity for low amplitudes ($V_{ac} \ll V_T$) reflects the dynamical response of the pinned CDW mode, with possible contributions also coming from the depinned (sliding) CDW as discussed below. We will compare our experiments to the predictions of both the classical and the tunneling models.

A phenomenological description of the pinned CDW by Lee, Rice, and Anderson[16] assumes that the response is classical, and can be described by the response of a damped classical oscillator in the presence of an ac driving field

$$\frac{d^2x}{dt^2}+\frac{1}{\tau}\frac{dx}{dt}+\omega_0^2 x=\frac{eE}{M}e^{i\omega t}, \tag{3}$$

where M is the mass of the CDW (which can be associated with the Fröhlich mass), $\tau=M/\Gamma$ where Γ is the damping constant, and $\omega_0^2=k/M$ with k the restoring force. Equation (3) leads to a conductivity as follows:

$$\mathrm{Re}\sigma(\omega)=\frac{ne^2\tau}{M}\left[1+\frac{\tau^2}{\omega^2}(\omega_0^2-\omega^2)^2\right]^{-1}, \tag{4a}$$

$$\mathrm{Im}\sigma(\omega)=\frac{ne^2}{M}\frac{(\omega_0^2-\omega^2)\tau^2}{\omega}\times\left[1+\frac{\tau^2}{\omega^2}(\omega_0^2-\omega^2)^2\right]^{-1}, \tag{4b}$$

where n is the effective charge density.

For a weakly damped system $\mathrm{Re}\sigma(\omega)$ has a peak and $\mathrm{Im}\sigma(\omega)$ a zero crossing at $\omega=\omega_0$, and the sharpness of the peak in $\mathrm{Re}\sigma(\omega)$ is determined by $1/\tau$. For an overdamped system with $\omega \ll \omega_0$, $\mathrm{Re}\sigma(\omega)$ smoothly increases from $\mathrm{Re}\sigma(\omega)=0$ at $\omega=0$ to

$$\mathrm{Re}\sigma(\omega\rightarrow\infty)=\frac{ne^2\tau}{M}$$

and $\mathrm{Im}\sigma(\omega)$ has a maximum. The crossover (co) frequency is determined by $\omega_{co}=\omega_0^2\tau$. The response of a weakly and strongly damped system is shown in Fig. 8.

Comparing the observed frequency dependence shown in Fig. 4 with the response expected for a weakly and strongly damped system, it is evident

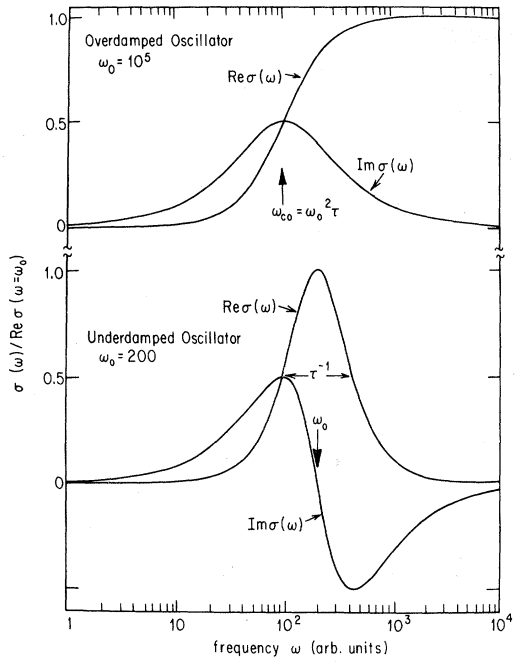

FIG. 8. Real and imaginary parts of the conductivity, Re$\sigma(\omega)$ and Im$\sigma(\omega)$, as calculated for an overdamped and underdamped classical harmonic oscillator [see Eq. (4)].

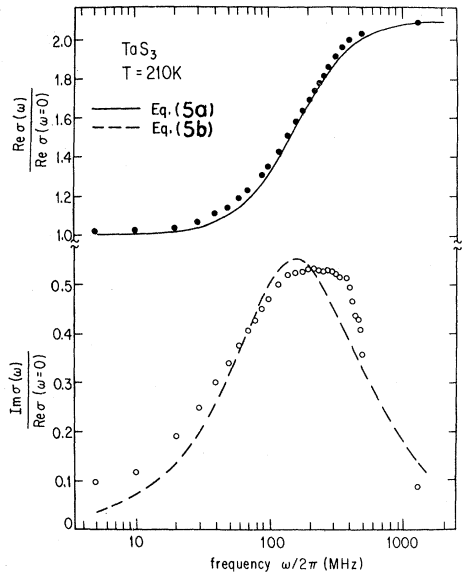

FIG. 9. Re$\sigma(\omega)$ and Im$\sigma(\omega)$ measured for TaS_3 at $T=210$ K. The solid and dotted lines are fits to the classical overdamped oscillator model, with parameters given in the text.

that in the framework of a classical description, the CDW response is overdamped. In this limit,

$$\mathrm{Re}\sigma(\omega)=\frac{ne^2\tau}{M}\frac{1}{1+(\omega_{co}/\omega)^2}\ ,$$

$$\mathrm{Im}\sigma(\omega)=\frac{ne^2\tau}{M}\frac{\omega_{co}}{\omega}\frac{1}{1+(\omega_{co}/\omega)^2}\ ,$$

at frequencies $\omega<\omega_0$.

We have fitted the measured Re$\sigma(\omega)$ and Im$\sigma(\omega)$ to Eq. (3.3) and find a reasonable agreement. This is shown in Fig. 9, with chosen parameters $\omega_{co}/2\pi=160$ MHz and $ne^2\tau/M=1.1\sigma_{dc}$.

Equation (5b) also leads to a low-frequency dielectric constant, which, if one includes the dielectric constant of the uncondensed electrons, is given by

$$\epsilon-1=\frac{2}{3}\frac{\hbar^2\omega_P^2}{\Delta^2}+\frac{\Omega_P^2}{\omega_0^2}\ , \tag{6}$$

where the first term is the dielectric constant of a one-dimensional semiconductor with a single-particle gap Δ, and $\omega_p=(4\pi ne^2/m)^{1/2}$ is the plasma frequency. The second term is the contribution from the pinned mode, with $\Omega_p^2=4\pi ne^2/M$. With the pinned mode neglected, and using $\Delta=700$ K, as evaluated from the temperature dependence of the low-field dc conductivity, and with $\omega_p\approx 1$ eV, characteristic of a narrow-band semiconductor, one obtains $\epsilon\approx 10^2$ orders of magnitude smaller than the measured value. With the use of Eq. (6), and a Fröhlich mass $M=10^3$ m and $n=10^{21}$ cm^{-3}, we obtain a pinning frequency $\omega_0=2\times 10^{10}$ sec^{-1}.

The real and imaginary part of the conductivity can be combined to give

$$\omega\frac{\mathrm{Re}\sigma(\omega\to\infty)}{\mathrm{Im}\sigma(\omega\to 0)}=\omega_0^2\tau=\omega_{co}\ , \tag{7}$$

and from the measured high-field conductivity and low-frequency dielectric constant we obtain $\omega_{co}=277$ MHz which compares favorably with the crossover frequency obtained from the measured frequency dependence alone.

We conclude therefore, that a classical description of the pinned CDW mode gives a good account of the measured frequency-dependence response over a broad frequency range, with a consistent description of the parameters involved. The response of the CDW is strongly overdamped in this model.

Next we compare our experiments with the pre-

diction of the tunneling model, which—as we have shown in I—gives an excellent quantitative description of the detailed form of the field-dependent conductivity. Our discussion of $\sigma(\omega)$ will closely follow the discussion of $\sigma(\omega)$ and $\sigma(E)$ experiments performed in $NbSe_3$.[17] The model assumes that the CDW can tunnel across potential barriers, and a semiconductor model[4,5] was used to account for the field-dependent conductivity. The tunneling probability $P(E)$ evaluated for CDW tunneling leads to a field-dependent conductivity,

$$\sigma(E)=A\left[1-\frac{E_T}{E}\right]\exp\left[\frac{-E_0}{E}\right], \tag{8}$$

where A is a constant of proportionality,

$$E_0=\frac{\pi\epsilon_g^2}{4he^*v_F},$$

where ϵ_g is the gap across which the CDW's have to tunnel, and $e^*/e=m/M_F$. The threshold field is given by $E_T=\epsilon_g/e^*L$, where L is the correlation length of the CDW. Equation (8) gives an excellent account of $\sigma(E)$ with $E_T=1.3$ V/cm and $E_0=5E_T$.

The frequency-dependent conductivity has two contributions in this model, one coming from the tunneling CDW's and the other from the response of the pinned mode. To evaluate the first contribution, a model developed for superconductor-insulator-superconductor (SIS) junctions by Tucker[18] was used to obtain the frequency-dependent conductivity. For a small-amplitude ac excitation the theory leads to a direct scaling between the field- and frequency-dependent conductivity,

$$\sigma^t(\omega/\omega_T)=\sigma(E/E_T), \tag{9}$$

where σ^t refers to the tunneling contribution of $\sigma(\omega)$, and $\hbar\omega_T=E_Te^*L$. The energy $\hbar\omega_T$ is associated with the energy gap $\hbar\omega_p$.

In Fig. 10 we show both $\sigma(\omega)$ and $\sigma(E)$ with the voltage and frequency scales adjusted to show the scaling relation. It is apparent from Fig. 10 that Eq. (9) is obeyed at frequencies corresponding to $E>3E_T$, while below this frequency range $\sigma(\omega)>\sigma(E)$ suggesting an extra contribution to the frequency-dependent conductivity. The scaling relation [Eq. (9)] and Fig. 10 lead to a threshold frequency $\omega_T/2\pi=25$ MHz. Associating this frequency with the pinning gap $\epsilon_g=\hbar\omega_p$ leads to $\epsilon_g=16\times10^{-20}$ ergs, or 0.11 K, orders of magnitude smaller than the thermal energy kT.

The low-frequency contribution to the frequency-dependent conductivity arises in this

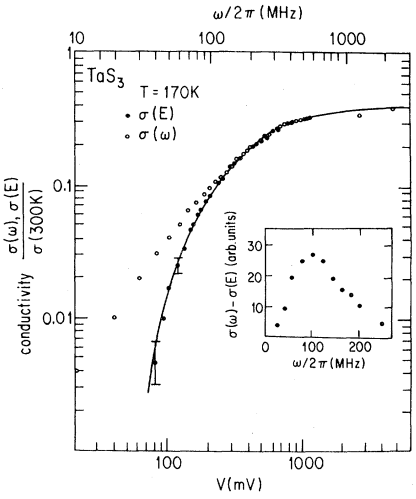

FIG. 10. $\sigma(\omega)$ and $\sigma(E)$ in TaS_3 at $T=170$ K. The inset shows $\sigma(\omega)-\sigma(E)$, which may represent the pinned-mode contribution $\sigma^P(\omega)$ (see text).

model from the response of the pinned mode. Adopting a classical approach [also used to describe $\sigma(\omega)$ for a semiconductor], Eq. (3) leads to the pinned-mode contribution,

$$\sigma^P(\omega)=\sigma^P(\omega_T')\frac{\omega^2/\tau^2}{(\omega_T'^2-\omega^2)^2-\omega^2\tau^2}. \tag{10}$$

The frequency-dependent conductivity then may be represented as the sum of the tunneling and pinning-mode contribution,

$$\sigma(\omega)=\sigma^t(\omega)+\sigma^P(\omega), \tag{11}$$

with $\sigma^t(\omega)$ given by Eq. (8) and $\sigma^P(\omega)$ by Eq. (10). In the inset of Fig. 10 we have plotted $\sigma(\omega)-\sigma^t(\omega)$, with $\sigma^t(\omega)$ given by a scaling relation. $\sigma^P(\omega)$ looks like a damped response of a pinned mode, and a fit to Eq. (10) leads to $\omega_T'=100$ MHz and $\omega_T\tau\approx1$. In the phenomenological description ω_T', which determines the frequency dependence of the pinned mode, is the same as ω_T, the threshold frequency obtained from the scaling of the field and frequency dependence as shown in Fig. 10. There we obtain $\omega_T'\approx4\omega T$. We note that in $NbSe_3$, $\omega_T'\sim\omega_T$ in both CDW phases.[17] Also in $NbSe_3$, E_0 is close to E_T while in TaS_3, $E_0=5E_T$. Whether a more complete description which includes the clear distinction between the pinning gap $\hbar\omega_T$ and the energy $\hbar\omega$ associated with E_0 leads to a difference between ω_T' and ω_T remains to be seen. Also, this discrepancy may be the consequence of the model, where the tunneling across potential barriers is modeled by a gap in the CDW excitation spectrum.

TABLE I. Parameters which characterize the field- and frequency-dependent transport in TaS_3 in the coherent CDW state and in $NbSe_3$. The data presented for $NbSe_3$ is for very pure samples with a high residual resistivity ratio.

	E_T (V/cm)	E_0 (V/cm)	ϵ	$\omega_0^2\tau/2\pi$[a] (MHz)	$\omega_T/2\pi$ (MHz)	$\epsilon g=\hbar\omega_T$ (10^{-20} erg)	L[b] (μm)	$2\xi_0$[c] (μm)
TaS_3 $T=170$ K	2.2	0.11	10^7	240	25	16.5	0.5	0.13
$NbSe_3$ $T=130$ K	0.110	0.22	3×10^7	50	11	7.4	5	5
$NbSe_3$ $T=42$ K	0.012	0.024	2×10^8	45	3.5	2.3	12	12

[a]Obtained from $\sigma(\omega)$.
[b]Using $L=\epsilon_g/(e^*E_T)$ and $e^*/e=m/M_F=10^{-3}$.
[c]From $E_0=E_T[1+L/(2\xi_0)]$.

The parameters, obtained by fitting $\sigma(\omega)$ and $\sigma(E)$ to the classical and to the tunneling model, are collected in Table I. The correlation length L was calculated using $L=\epsilon_g/e^*E_T=\hbar\omega_T/e^*E_T$ with $e/e^*=m/M_F=10^{-3}$, and the coherence distance ξ_0 was obtained from the relation

$$E_0=E_T\left[\frac{L}{2\xi_0}+1\right].$$

Both L and ξ_0 represent enormous length scales. The number of electrons per chain corresponding to L and ξ_0 is of the order of 10^3.

As the CDW's on the neighboring chains become correlated, the ω- and E-dependent conductivity represents the response of correlated CDW segments, and the number of electrons involved in the coherent response is much more than the number given above.

Our experiments involving the joint application of dc and ac fields will be described in a separate publication. Here we only mention one phenomenon, called photon-assisted tunneling, which is predicted by the tunneling model. Aside from the ac conductivity for low-amplitude ac fields, the tunneling model[4] also makes specific predictions of the response in the presence of ac and dc fields. The consequence of the quantum aspects of the theory is that the energy $\hbar\omega$ may be combined with the energy e^*EL provided by the dc field. In particular, for a joint ac and dc driving voltage of the form $V=V_{dc}+V_{ac}\cos\omega t$, one expects from the classical description no excess dc conductivity unless $V_{dc}+V_{ac}>V_T$. In the tunneling model, however, even for $V_{dc}+V_{ac}<V_T$, the energy quantum $\hbar\omega/e^*$ can span the difference between V_{dc} and V_T, leading to a dc conductivity when $V_{dc}+\hbar\omega/e^*>V_T$.

We have searched for this photon-assisted tunneling using various combinations of ac and dc fields and ac frequencies. With a sensitivity more than 2 orders of magnitude larger than the excess dc conductivity predicted from the tunneling theory we did not observe photon-assisted tunneling phenomena.

We conclude, therefore, that the tunneling model gives a good account for the field- and frequency-dependent conductivity, but fails when both ac and dc excitations are applied to the sample. The reason for this discrepancy (which may be due to the simplified description of the quantum-mechanical model) has been discussed by Bardeen.[5] Another possibility for the failure to observe photon-assisted tunneling is the presence of time-dependent effects associated with the development of the collective current carrying mode. These have been observed in $NbSe_3$,[19] and are most probably also associated with the CDW phenomena in TaS_3.

C. Disordered CDW state at low temperatures

Below about $T=100$ K there is no evidence for a sharp threshold field for the onset of nonlinear conduction and we do not observe sharp peaks in the noise spectrum.[20] We suggested in I that at low temperatures the coherent response of the CDW state is absent and we called this state the disordered CDW state.

The most simple representation of the response due to external ac excitations would be to assume that different CDW regions are pinned with different pinning energies $\hbar\omega_p$, and that the

frequency-dependent conductivity is the sum of frequency-dependent responses of different CDW regions. Such a model has already been worked out by Portis[21] to account for the frequency-dependent response of the CDW in $NbSe_3$. The consequence of this distribution is a smearing of the frequency-dependent response and a smooth increase of σ with ω, in contrast to the rapid frequency dependence given by Eq. (11).

This effect has been discussed recently from a microscopic point of view by Feigelman and Vinoleus.[22] They have shown that in the presence of backscattering impurities the CDW leads to a frequency-dependent response,

$$\sigma(\omega)=\frac{ne^2\tau}{m^*}(\omega\tau)^2\ln^2(\omega\tau)\ , \tag{12}$$

at low frequencies. Equation (12) has the same form that was obtained for the frequency-dependent conductivity for localized single-particle states and is called the Mott-Berezinsky law.[23] There, τ is a characteristic time associated with the localization.

A good approximation of Eq. (12) is a simple power law,

$$\sigma(\omega)=A\omega^{\alpha}\ , \tag{13}$$

with $\alpha<1$ at low frequencies. In Fig. 11 we show the frequency-dependent conductivity $\mathrm{Re}\sigma(\omega)$ measured at 90 K. The full line is Eq. (13) with $\alpha=0.27$. It is evident that Eq. (13) leads to a good description of the low-frequency conductivity over 2 orders of magnitude. [In case of frequency-dependent conductivity observed in materials where single-particle localization occurs, either $\sigma(\omega)$ or $\sigma(\omega)-\sigma(\omega=0)$ (i.e., the excess frequency-dependent conductivity) is plotted. Here $\sigma(\omega=0)$ is small at 90 K, and a plot of $\sigma(\omega)-\sigma(\omega=0)$ is close to $\sigma(\omega)$ displayed in the figure, and only low-frequency ($f\leq 10$ MHz) points are strongly affected.]

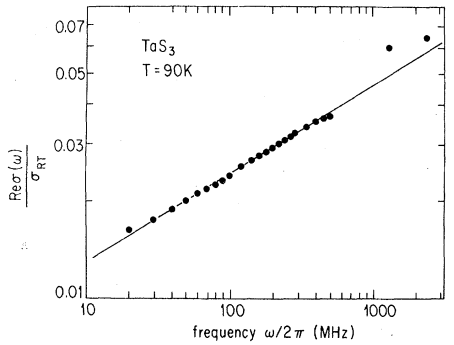

FIG. 11. Frequency dependence of the conductivity of TaS_3 at $T=90$ K. The full line is a fit to Eq. (13), with $\alpha=0.27$.

An obvious shortcoming of the model is that it does not take finite-temperature effects into account, and therefore the temperature does not appear explicitly in Eqs. (12) and (13). In the case of localized single-particle states the power law is observed over a wide temperature range with α slowly decreasing and A increasing with increasing temperature. Owing to experimental limitations associated with the large sample resistance, we were not able to measure the frequency-dependent conductivity in this temperature region.

We also note that because the same frequency dependence is predicted *both* for single-particle states localized by disorder,[24] and by a random localization of CDW's by impurities, the observed frequency dependence may also arise from impurity states in the gap region. Indeed, we have argued in I that the flattening off of the low-field dc conductivity at low temperatures is due to impurity states which contribute to the dc transport at low temperatures, where only a small number of thermally excited states participate in the transport. These impurity states can also give rise to a $\sigma(\omega)$ as given by Eqs. (12) and (13) and shown in Fig. 10. Detailed studies on $\sigma(T,\omega)$ in this region may clarify the role of single-particle states and electrons condensed into the CDW state. We note, however, that localized single-particle states do not lead to a conductivity which strongly depends on the applied electric field. The account, therefore, for both $\sigma(\omega)$ and $\sigma(E)$, the effect of the CDW has to be considered.

V. COMPARISON OF THE TaS_3 and $NbSe_3$

In I we have compared the field-dependent conductivity observed in the coherent CDW state with nonlinear effects measured in the linear-chain compound $NbSe_3$. In both materials a tunneling formula describes $\sigma(E)$ over a broad electric field range. The characteristic fields E_0 and E_T are very small in the low-temperature ($T<59$ K) CDW state of $NbSe_3$, where both parameters are approximately 2 orders of magnitude smaller than in TaS_3 below T_p. The upper CDW state of $NbSe_3$ is characterized by a field dependence between these two cases.

The ω-dependent response is also very similar in $NbSe_3$ (Refs. 17, 25, and 26) and TaS_3 in the coherent CDW region. In both compounds $\mathrm{Re}\sigma(\omega)$ smoothly increases with ω and $\mathrm{Im}\sigma(\omega)$ shows a

maximum at frequencies where $\mathrm{Re}\sigma(\omega)$ shows the strongest dependence. In terms then of a classical model, the CDW response is strongly overdamped. A tunneling model also describes $\sigma(\omega)$ in both compounds. There is also a strong correlation between the field- and frequency-dependent transport in both compounds. Broadly speaking, the low-frequency dielectric constant is inversely proportional to restoring forces associated with the potential in which the CDW is pinned, and the threshold field is proportional to this potential. From this crude argument one expects that ϵE_T is approximately constant. In Table I we have collected the measured ϵ and E_T values for both CDW phases of $NbSe_3$ and for TaS_3. ϵE_T is indeed approximately the same for all three CDW phases as expected from the above argument. This strongly suggests that the pinning and subsequent depinning mechanism is the same in $NbSe_3$ and TaS_3, and the difference in dimensionality and the absence of presence of uncondensed electrons does not play a fundamental role in the CDW dynamics.

We have also remarked the difference between the temperature dependence of $\sigma(E)$ in TaS_3 and $NbSe_3$. In both CDW phases of $NbSe_3$ the characteristic fields E_0 and E_T diverge at the Peierls transition, while the field-dependent conductivity is independent of T up to T_p in TaS_3. This difference also shows up in the ω-dependent transport studies in TaS_3 and $NbSe_3$. The ω-dependent response moves to progressively higher frequencies when T_p is approached from below in both CDW phases in $NbSe_3$,[25,18] and also $\epsilon \rightarrow 0$ at the Peierls transition.[25] In contrast to this, in TaS_3 both $\sigma(\omega)$ and ϵ are independent of T below T_p. Thus, the temperature dependence of $\sigma(\omega)$ and $\sigma(E)$ are strongly correlated in both compounds.

The reason why both $\sigma(E)$ and $\sigma(\omega)$ suggest higher pinning energies in TaS_3 than in $NbSe_3$ is not clear. If in TaS_3 the CDW is commensurate with the lattice, then the large pinning energies suggest that pinning is dominately due to commensurability. Alternatively, TaS_3 may reflect the stronger pinning by impurities or less pure specimens. Experiments on TaS_3 with various amounts of impurities may clarify this question.

VI. CONCLUSION

We have observed field- and frequency-dependent conductivity associated with the development of the Peierls-Fröhlich CDW state in the highly anisotropic conductor, orthorhombic TaS_3.

A phase diagram which demonstrates the various phenomena which are associated with the progressive buildup of CDW correlations is shown in Fig. 12. At high temperatures ($T > 300$ K) there is no evidence for 1D CDW's. The conductivity is high and shows metallic behavior, and it is independent

Orthorhombic TaS_3

Disordered CDW	Coherent CDW	1D Resistive Fluctuations	Metallic
Commensurate superstructure (x rays)	commensurate superstructure (x rays)	CDW fluctuations (1D diffuse x rays)	
Disorderlike low field σ_{dc}	activated low-field behavior $\sigma_{dc}=Ae^{-\Delta/kT}$	nonmetallic $\sigma(T)$	$\sigma_{RT}\approx 2.6\times 10^3\ \Omega^{-1}\,\mathrm{cm}^{-1}$ Anisotropic $\sigma/\sigma_\perp \sim 10^2$
Strongly nonlinear $\sigma_{dc}=\sigma(E)$. No sharp threshold	strongly nonlinear $\sigma_{dc}=\sigma(E)$ sharp threshold E_T	ohmic $\sigma_{dc}\neq\sigma(E)$.	
Large dielectric constant	huge dielectric constant $\epsilon \sim 10^7$	positive dielectric constant $\epsilon > 0$	
MHz frequency dependence $\sigma(\omega)\sim\omega^\alpha$	MHz frequency dependence $\sigma_{ac}=\sigma(\omega)$	microwave frequency dependence $\sigma_{ac}=\sigma(\omega)$	
no narrow-band noise	narrow-band noise for $E > E_T$	no narrow-band noise	

~100 K $T_P=215$ K ~270 K

Temperature

FIG. 12. CDW regions in TaS_3 as established from temperature, field- and frequency-dependent conductivity studies. The x-ray observations are from Ref. 9.

of frequency with no out-of-phase component, as expected for a metal where current is carried by extended electron states. Below 300 K the progressive buildup of 1D CDW's leads to a strong supression of the conductivity, suggesting resistive fluctuations and associated localization effects, as evidenced by a frequency-dependent conductivity and positive dielectric constant. These may reflect single-particle localization effects on the dynamical response of the CDW mode in the fluctuating region. We note that the situation here is different from that observed in the organic conductor tetrathiafulvalene-tetracyanoquinodimethane (TTF-TCNQ),[12] were in the 1D fluctuating CDW region ($T > 56$ K) the conductivity strongly increases with decreasing temperature.

At $T = 215$ K a phase transition in orthorhombic TaS_3 occurs to a 3D-ordered CDW state. Strongly nonlinear conductivity with a sharp threshold field, and narrow-band noise phenomena point to a coherent CDW response. In other words, the whole sample responds to external ac or dc driving fields in a highly coherent manner. The frequency-dependent conductivity suggest small pinning energies (per electron), and provides direct evidence for a collective mode which involves a large number of condensed electrons. While a classical description[13,14] accounts for the qualitative features of $\sigma(E)$ and $\sigma(\omega)$, a tunneling model[4,5] provides a detailed fit to both the field and frequency dependence. Attempts to provide other evidences for quantum effects, however, like photon-assisted tunneling, were unsuccessful. At low temperatures there is no evidence for a coherent CDW response. While impurity states may also lead to ω-dependent response in this temperature region, the observed field dependence suggest that incoherent response of various CDW segments play an important role in this so-called disordered CDW state. The ac-dc coupling experiments and detailed noise measurements performed in the temperature region where a coherent CDW response is observed will be reported later.

ACKNOWLEDGMENTS

We wish to thank A. H. Thompson for providing the TaS_3 samples ued in this study. We also acknowledge various discussions on CDW phenomena with J. Bardeen, M. Weger, T. Holstein, and W. G. Clark. This research was supported by the NSF Grant No. DMR 81-03085. One of us (A.Z.) received support from an IBM Fellowship.

[1]A. Zettl, G. Grüner, and A. H. Thompson, preceding paper, Phys. Rev. B 26, 5760 (1982).
[2]H. Fröhlich, Proc. Roy. Soc. London Ser. A 223, 296 (1954).
[3]G. Grüner, *Comments in Solid State Physics* (in press).
[4]John Bardeen, Phys. Rev. Lett. 45, 1978 (1980).
[5]John Bardeen, in Proceedings of the International Conference on Low Dimensional Conductors, Boulder, Colorado, 1981 [Mol. Cryst. Liq. Cryst. 81, 1 (1982)].
[6]C. M. Jackson, A. Zettl, G. Grüner, and A. H. Thompson, Solid State Commun. 39, 531 (1981).
[7]A. Zettl and G. Grüner, Phys. Rev. B 25, 2081 (1982).
[8]L. I. Buravov and I. F. Shchegolev, Prib. Tekh. Eksp. 14, 171 (1971) [Instrum. Exp. Tech. (USSR) 14, 528 (1971)].
[9]T. Sambongi, T. Tsutsumi, Y. Shiozaki, M. Yamamoto, D. Yamaya, and Y. Abe, Solid State Commun. 22, 729 (1977); K. Tsutsumi, T. Sambongi, S. Kagoshima, and T. Ishiguro, J. Phys. Soc. Jpn. 44, 1735 (1978).
[10]G. Grüner, A. Jánossy, K. Holczer, and G. Mihály, in *Quasi-one-dimensional Conductors I,* Vol. 95 of *Lecture Notes on Physics,* edited by S. Barisic, A. Bjelis, J. R. Cooper, and B. Leontic (Springer, New York, 1979), p. 246.
[11]S. Alexander, J. Bernasconi, W. R. Schneider, R. Biller, W. G. Clark, G. Grüner, R. Orbach, and A. Zettl, Phys. Rev. B 24, 7474 (1981).
[12]A. J. Heeger, in *Highly Conducting One Dimensional Solids,* edited by J. T. Devreese, R. P. Evrard, and V. E. van Doren (Plenum, New York, 1979), p. 69.
[13]G. Grüner, A. Zawadowski, and P. M. Chaikin, Phys. Rev. Lett. 46, 511 (1981).
[14]G. Grüner, in Proceedings of the International Conference on Low Dimensional Conductors, Boulder, Colorado, 1981 [Mol. Cryst. Liq. Cryst. 81, 17 (1982)].
[15]A. Zettl, G. Grüner, and A. H. Thompson, Solid State Commun. 39, 899 (1981).
[16]P. A. Lee, T. M. Rice, and P. W. Anderson, Solid State Commun. 14, 703 (1974).
[17]G. Grüner, A. Zettl, W. G. Clark, and John Bardeen, Phys. Rev. B 24, 7247 (1981).
[18]J. R. Tucker, IEEE J. Quant. Electron. 15, 1234 (1979).
[19]N. P. Ong (unpublished); J. C. Gill, Solid State Commun. 39, 1203 (1981); R. M. Fleming, *ibid.* Solid State Commun. 43, 167 (1982); A. Zettl and G. Grüner, Phys. Rev. B 26, 2298 (1982).
[20]G. Grüner, A. Zettl, W. G. Clark, and A. H. Thompson, Phys. Rev. B 23, 6813 (1981).
[21]A. M. Portis, in Proceedings of the International

Conference on Low Dimensional Conductors, Boulder, Colorado, 1981 [Mol. Cryst. Liq. Cryst. 81, 59 (1982)].
[22]M. V. Feigelman and V. M. Vinokur, Phys. Lett. 87A, 53 (1981).
[23]N. F. Mott and E. A. Davis, *Electronic Processes in Non-Crystalline Materials* (Clarendon, Oxford, 1971).
[24]S. Alexander, J. Bernasconi, W. R. Schneider, and R. Orbach, Rev. Mod. Phys. 53, 175 (1981).
[25]G. Grüner, L. C. Tippie, J. Sanny, W. G. Clark, and N. P. Ong, Phys. Rev. Lett. 45, 935 (1980).
[26]S. W. Longcor and A. M. Portis, Bull. Am. Phys. Soc. 25, 340 (1980).